Colloid Polym Sci 277:306–317 (1999)

ORIGINAL CONTRIBUTION

N. Hattori
M. Hara
H. Okabayashi
C.J. O'Connor

Raman scattering spectra and molecular conformations of bis(quaternaryammonium bromide)-water systems

Received: 21 July 1998
Accepted in revised form: 9 November 1998

N. Hattori · M. Hara · H. Okabayashi (✉)
Department of Applied Chemistry
Nagoya Institute of Technology
Gokiso-cho, Showa-ku
Nagoya 466-8555, Japan
e-mail: okabayas@ach.nitech.ac.jp
Tel.: +81-52-7355212
Fax: +81-52-7355247

C.J. O'Connor
Department of Chemistry
The University of Auckland
Private Bag 92019, Auckland
New Zealand

Abstract The dimeric bis(quaternaryammonium bromide) surfactants, $[Br^-(CH_3)_2N^+(C_mH_{2m+1})—(CH_2)_s—(C_mH_{2m+1})N^+(CH_3)_2Br^-$, $s = 2$, 3 and $m = 4$, 6, 10 and 12, $s = 6$ and $m = 8$, 10, 12], have been synthesized and the phase maps of the sm6-8-water, sm6-10-water and sm6-12-water binary systems have been determined (sm6-8 implies $s = 6$, $m = 8$). In order to examine the molecular structures of these solid samples and of their dimeric surfactant-water binary systems, Raman spectra of the simple dimeric surfactants, sm2-4 and sm3-4, in which crystal structures of the trans- and cis-type conformations have been determined by single-crystal X-ray diffraction analysis, have been investigated, and Raman bands characteristic of these skeletal structures were found in the skeletal deformation region. On the basis of these characteristic Raman bands for the two conformations, it has been concluded that the dimeric surfactants, sm6-8, sm6-10 and sm6-12 also take up a cis-type conformation in the crystalline state. Furthermore, it has been found that the Raman bands in the C—H stretching, skeletal stretching and CH_2 scissoring regions are sensitive to phase structure.

Key words Raman spectra – Bis(quaternaryammonium bromide) – Phase-structure

Introduction

Considerable attention has been paid to morphological studies on homologous series of bis(quaternaryammonium bromide) surfactants [dimeric surfactants (DS)][1–17]. These molecules are composed of two *n*-alkyldimethylammonium bromide moieties whose polar head groups are chemically connected in pairs by an alkanediyl chain (referred to as a spacer). This dimerization brings about variations in physico-chemical properties compared with those of the original surfactant molecules. In particular, it is well known that the length of the spacer markedly affects the morphology of an aggregate. Zana and Talmon [14] used transmission electron microscopy to investigate the microstructures formed by the DS with acyl carbon chain number $m = 12$ and the number of spacer methylene units $s = 2$, 3 or 4 in aqueous solution. The results indicated that the DS with a short spacer ($s = 2$, 3) form long, thread-like and entangled micelles, even at low concentrations, while the DS molecules with $s = 4$ form spheroidal micelles. Thus, short spacers obviously promote lower spontaneous curvature in the assemblies.

Hirata and coworkers [17] investigated the microstructure of the self-assembly systems of some DS by small-angle neutron scattering and found that for the DS with a short spacer ($s = 2$) both micellar growth and shape variation were more pronounced, while for the DS with a long spacer ($s = 6$) the extent of micellar growth and shape variation became very small.

The results of Alami et al. [15] imply that variation in the morphology of an aggregate formed by the DS strongly depends on the specific area per surfactant molecule which, in turn, is influenced by the length of the spacer. Indeed, Diamant and Andelman [16] pointed out that the small specific area imposed by short spacers

may lead to a large packing parameter thereby accounting for the formation of cylindrical micelles, while the close-to-maximum areas imposed by the presence of a medium spacer explains the spherical shape. Furthermore, they presented a theoretical explanation for the experimental results of Zana and Talmon [14] and Alami et al. [15].

The packing property of self-assembly systems seems to depend on many factors. In order to discuss quantitatively the relationship between geometrical packing parameters and morphological characteristics, the conformational change brought about by the self-assembling of surfactant molecules must be investigated in detail, since the packing parameters will be changed by variation in the conformation of these molecules.

In their Raman scattering studies of surfactant-water binary systems Okabayashi and coworkers [18–27] have already demonstrated that a conformational change of surfactant molecules occurs upon micellization. Micellization brings about preferential stabilization of a specific rotational isomer, leading to variation in the packing parameter. It is therefore clear that further understanding of the relationship between the geometrical packing parameter and the morphology of a DS-water system would be obtained by a conformational study of the DS in the solid state and in aqueous solution. However, very little is known of conformational studies of DS using Raman scattering spectra.

In this study, a series of DS and their simple related compounds have been synthesized and investigated by using Raman scattering spectroscopy. The conformations of the DS in the solid state and in various aqueous phases are then discussed.

Experimental

Materials

Bis(quaternaryammonium bromide) surfactants (DS) of general formula

$$Br^-(CH_3)_2\overset{+}{N}-(CH_2)_s-\overset{+}{N}(CH_3)_2\,Br^-$$
$$\qquad\qquad\quad C_mH_{2m+1}\qquad C_mH_{2m+1}$$

were synthesized as follows [9, 10]. The reaction of *N*,*N*,*N*′,*N*′-tetramethyl-1,6-diaminohexane (b.p. = 57.1–58.1 °C) with the correspondence *n*-alkylbromide was performed in dried ethanol under reflux ($T = 353$ K) for 48 h in the presence of a 5–10% excess of *n*-alkylbromide, in order to ensure as complete bisquaternization as possible. The DS thus prepared (Table 1) were recrystallized in various solvent mixtures (ethanol-ethylacetate or acetone-ethylacetate). Sample identity was confirmed by NMR and elemental analysis; the agreement between calculated and observed values was within ±0.5% (Table 1). Since the observed elemental analysis data for the DS D_0(sm6-3) (which was very hygroscopic) were in disagreement with the calculated values, identification of the sample was carried out by ^1H and ^{13}C NMR spectroscopy. Abbreviations for the three series of DS thus prepared are also listed in Table 1. The reactants used for these syntheses, hexamethonium bromide [$(CH_3)_3N^+(CH_2)_6N^+(CH_3)_3 \cdot 2Br$, HMB] and *N*,*N*,*N*′,*N*′-tetramethyl-1,6-diaminohexane [$(CH_3)_2N(CH_2)_6N(CH_3)_2$, TMDH] were obtained from Wako Chemicals and Tokyo Kasei Kogyo, respectively, and all reactants were purified before reaction.

Table 1 Abbreviations of the dimeric surfactants (*DS*) and their elemental analysis data[a]

	Abbreviations		C%	H%	N%
A series	A1 (sm6-8)	Calcd.	55.91	10.47	5.02
		Found	55.53	10.72	4.68
	A2 (sm6-10)	Calcd.	58.62	10.82	4.56
		Found	58.51	11.14	4.45
	A3 (sm6-12)	Calcd.	60.88	11.12	4.18
		Found	60.66	11.51	4.05
B series	B1 (sm2-4 · $2H_2O$)[b]	Calcd.	39.45	8.99	6.57
		Found	39.76	9.42	6.33
	B2 (sm2-6 · H_2O)[b]	Calcd.	46.56	9.55	6.03
		Found	46.57	9.58	5.87
	B3 (sm2-10)	Calcd.	55.91	10.47	5.02
		Found	55.94	10.89	4.89
	B4 (sm2-12)	Calcd.	58.62	10.82	4.56
		Found	58.69	11.23	4.48
C series	C1 (sm3-4 · $1/2H_2O$)[b]	Calcd.	43.59	9.02	6.78
		Found	43.51	9.13	6.64
	C2 (sm3-6 · H_2O)[b]	Calcd.	47.70	9.69	5.85
		Found	47.44	9.91	5.66
	C3 (sm3-10 · H_2O)[b]	Calcd.	54.91	10.58	4.74
		Found	54.67	10.74	4.60
	C4 (sm3-12 · $2H_2O$)[b]	Calcd.	56.01	10.92	4.21
		Found	56.09	11.33	4.26
D	D_0 (sm6-3)	–	–	–	–

[a] sm2-4 implies that the number (*s*) of spacer methylene units is 2 and the number (*m*) of carbon atoms in the *n*-acyl chains is 4
[b] Calculated values for the hydrated *DS* including allowance for the water molecules of hydration

Phase map determinations and calorimetry

Sample solutions were prepared by placing the DS and H_2O components into glass ampoules, which were then sealed and the contents homogenized by annealing. The thermotropic transition temperature of the DS-H_2O system was determined with a differential scanning calorimeter (Rigaku DSC 8230), using a volatile pan with α-Al_2O_3 in the reference pan, at a scanning rate of 2 °C/min. The temperature dependence of the phase feature of the samples was determined by visual inspection as the ampoules were held in a temperature-controlled water bath (rate of temperature elevation and cooling 0.1 °C/min). The temperature was measured with a digital thermometer (Sato Keiryoki).

FT-Raman scattering measurements

Raman spectra below 4000 cm^{-1} were obtained with a Nicolet 950 Fourier transform Raman spectrometer using the Nd: YAG laser (CVI) excitation wavelength of 1064 nm with a resolution of 4 cm^{-1} at room temperature. Raman spectra of the solid samples were obtained from pressed solid samples in a capillary tube with a laser power of 400 mW. For measurements in the temperature

range −80 to 100 °C, samples were placed in a hand-made variable temperature system.

Light-scattering measurements

Light-scattering measurements were carried out on a Union Giken DLS 700 light-scattering photometer using He-Ne laser light (5 mW) at 632.8 nm. The refractive index increment of the sample solutions was measured on a Union Giken RM-102 differential refractometer at 633 nm. The temperature was kept at 20 ± 0.3 °C by circulating temperature-controlled water through the cell housings.

Results and discussion

This present study is mainly concerned with the molecular structures of DS in the solid state and various aqueous phases, as determined from the Raman scattering effect. The DS (A series) with a spacer of definite polymethylene chain-length [$(CH_2)_6$] were synthesized in order to determine the phase maps of the A series-H_2O binary systems. The simple DS (B and C series) with short spacers [$(CH_2)_s$, $s = 2$ and 3] were also synthesized to aid interpretation of the Raman scattering spectra of the A series. In particular, emphasis was focussed on the longitudinal accordion-like vibrational modes, as well as the skeletal stretch and C—H stretch modes, as a measure of the order of the *n*-octyl, *n*-decyl and *n*-dodecyl side chains and of the spacer chain.

The phase maps of the A series-H_2O binary systems are shown in Fig. 1. For the Al-H_2O system (Fig. 1A), the map consists of four regions (I, II, III and IV). A homogenous and transparent one-phase solution was obtained in region I, and in region II a homogeneous, transparent and viscous one-phase solution was obtained at higher temperatures, but this could be regarded as a gel phase at room temperature. It was found that region III is a coagel phase, while in region IV a coagel and a transparent gel coexist. For the A2-H_2O system (Fig. 1B), there exist three regions (I, II and III) which correspond to a homogenous and transparent one-phase solution, a gel (colorless, transparent and elastic) phase and a coagel phase, respectively. For the A3-H_2O system (Fig. 1C), in addition to a homogenous and transparent one-phase solution (region I), a gel phase (region II), a coagel phase (region III) and a (gel + coagel) phase (region IV), there exists a region V, in which hydrated crystals and an aqueous solution of A3 coexist and the two-phase system is in equilibrium.

For region I, which was obtained for all three systems, light-scattering measurements were carried out at various concentrations and the reduced scattering intensities were plotted against concentration. The results show that in this region there exists a critical

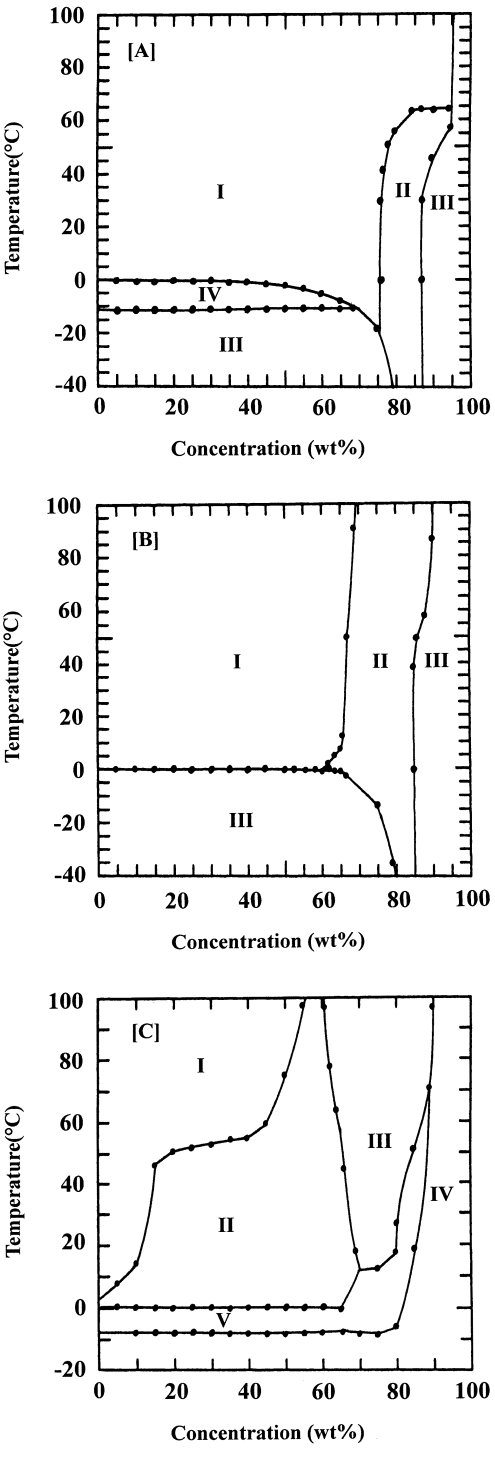

Fig. 1 A–C Phase maps for the A series-H_2O binary systems, **A**: Al-H_2O **B**: A2-H_2O and **C**: A3-H_2O (*filled circles*: transition temperature determined by calorimetric measurement). *Region I*: homogeneous and transparent one-phase solution; *region II*: homogeneous and transparent viscous one-phase solution; *region III*: coagel phase; *region IV*: coagel + transparent gel; *region V*: hydrated crystals + aqueous solution

micelle concentration (cmc), indicating the presence of a monomer-micelle equilibrium. The cmcs were 5.5×10^{-2} mol/l for A1, 8.1×10^{-3} mol/l for A2 and 1.8×10^{-3} mol/l for A3, values very close to those reported by Ikeda et al. [28], i.e. 7.3×10^{-2} (A1), 8.7×10^{-3} (A2) and 1.7×10^{-3} mol/l (A3), respectively.

For the A2-H_2O systems, we have already reported the existence of prolate micelles with an aggregation number of 24 in region I and that no micellar growth occurs [17].

The phase structures in regions II, III and IV and the structures of the solids are discussed below mainly by interpretation of the Raman spectra. Figure 2 shows the Raman spectrum of the solid A2 sample, in the region 600–1600 cm^{-1}, as a representative of the A-series samples. The frequencies of the observed Raman bands for the A series are listed in Table 2 together with a tentative assignment.

In order to examine the molecular conformations of the A series in the solid state, the Raman spectra of the simple DS (B and C series) with short methylene [$(CH_2)_2$ and $(CH_2)_3$] spacers were investigated. In particular, it was found that the Raman bands in the skeletal deformation region for these simple surfactants play an important role in determining the conformations of the A series. Moreover, the Raman bands coming from the skeletal C—C stretch and C—H stretch modes were found to be sensitive to the phase structures of the A series-H_2O binary systems.

Raman spectra of simple DS and their conformations

Schematic models of the molecular conformations for the B1 and C1 molecules, which we have previously determined by single-crystal X-ray diffraction analysis [29], are shown in Fig. 3. For the B1 molecule (Fig. 3A), the two *n*-butyl chains are in the trans configuration with respect to the extended N—$(CH_2)_2$—N skeleton, while those of C1 (Fig. 3B) are in the cis configuration. The methylene portions of the two *n*-butyl chains are in an extended form. The frequencies of the main Raman bands in the skeletal deformation region for B1 and C1 are listed in Table 3.

The difference in conformation between the B1 and C1 series was also strongly reflected in the Raman

Table 2 Raman bands frequencies (cm^{-1}) of the solid A series in the region 700–1500 cm^{-1}[a]

A1	A2	A3	Assignment (tentative)
1490 (w)	1490 (w)	1490 (w)	CH_3 deg. bend
1455 (vs)	1458 (vs)	1457 (vs)	CH_2 scis.
1445 (vs)	1443 (vs)	1441 (vs)	
1408 (m)	1410 (m)	1413 (m)	CH_2 wag.
1344 (w)	1343 (w)	1344 (w)	
1306 (m)	1302 (s)	1300 (s)	CH_2 wag., CH_2 twi.
1229 (w)	1230 (w)	1231 (w)	
1173 (w)	1175 (w)	1172 (w)	
1137 (w)	1136 (m)	1137 (m)	C—C str.
1120 (w)	1125 (m)	1126 (m)	
1080 (m)	1080 (m)	1081 (m)	
1065 (m)	1065 (s)	1067 (vs)	
1030 (m)	1030 (m)	1028 (m)	
985 (w)	990 (w)	980 (m)	C—C str., CH_2 rock
964 (w)	968 (m)	–	
950 (m)	–	–	
923 (w)	932 (w)	925 (w)	CH_2 rock
898 (m)	895 (m)	898 (m)	
764 (s)	767 (s)	767 (s)	C—N str.

[a] The frequencies of the very weak Raman bands have been omitted

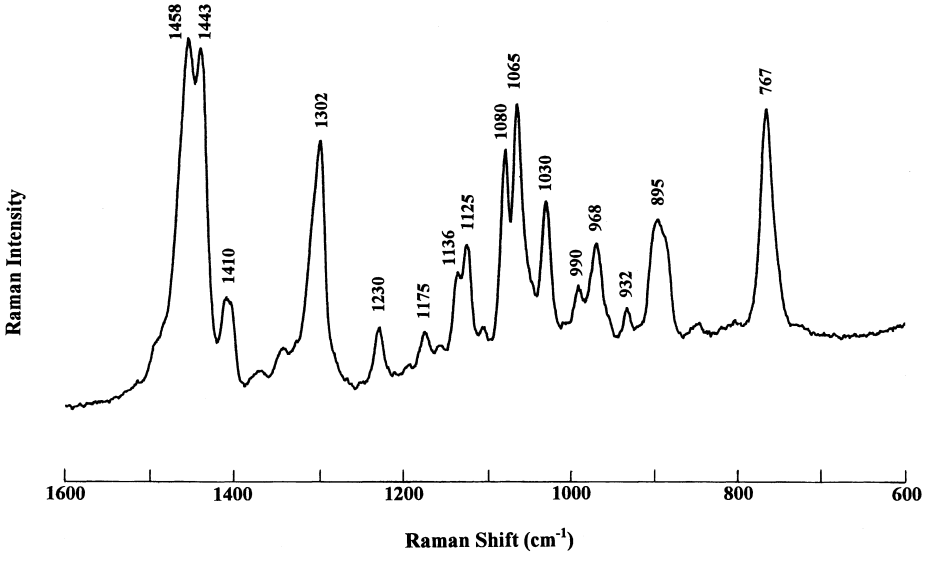

Fig. 2 Raman spectrum of the solid A2 sample in the 600–1000 cm^{-1} region

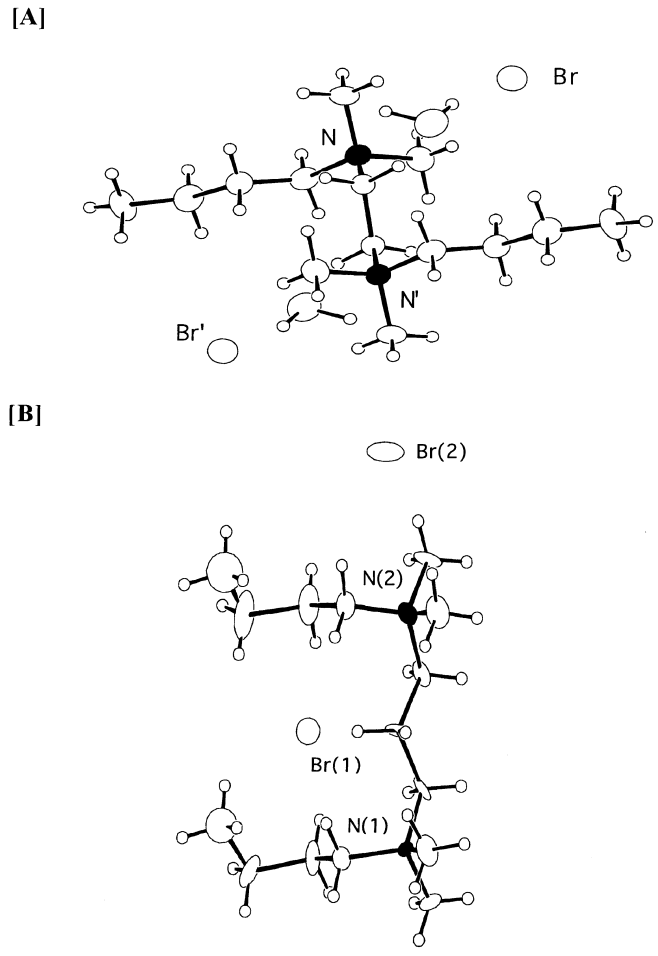

Fig. 3 A, B Schematic molecular conformational models [29] of **A** B1 and **B** C1 in the crystalline state

Table 3 Raman band frequencies of trans-type B1, cis-type C1 and of their related *DS* in the skeletal deformation region

DS		Band frequencies (cm^{-1})								
trans	B1		546			509	474		382	366
	B2		542			508	465		382	372
	B3		544			505	457		391	372
	B4		544			509	461		–	370
cis	C1	553		536	519		463	426		376
	C2	552		530	515		453	421		376
	C3	562		530	515		457	422		374
	C4	563		534	515		459	422		377

spectra. In particular, the vibrational bands in the region of the skeletal deformational modes provide direct information on the molecular conformation [30, 31]. The Raman spectra of the solid B1 and C1 samples in the skeletal deformation region are shown in Fig. 4. (The detailed normal mode analysis of B1 and C1 will be reported separately; however, it has been found that the

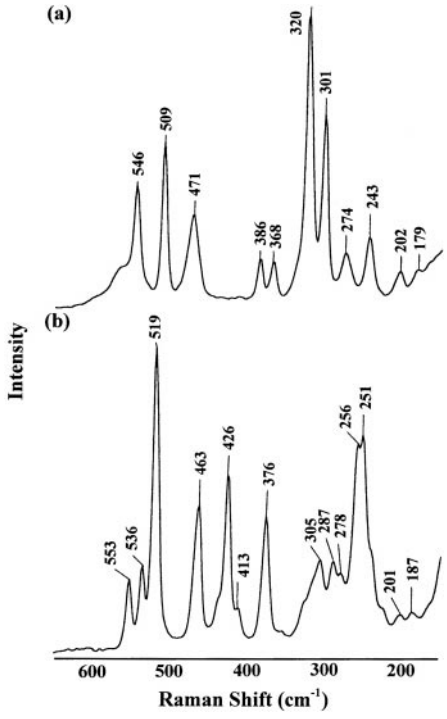

Fig. 4 a, b Raman spectra of the solid **a** B1 and **b** C1 samples in the skeletal deformation region at 25 °C

vibrational modes coupled among the CNC, CCN and CCC deformational modes are sensitive to the cis and trans configurations) It is now clear that the marked difference in the spectral features between the two simple DS must originate in the differences in their conformation. In particular, it should be noted that the Raman band at 423–426 cm^{-1}, observed for the crystalline C1 sample (Fig. 4b), disappears in the Raman spectrum of the crystalline B1 sample (Fig. 4a). Therefore, we may regard the band at 423–426 cm^{-1} as characteristic of the cis-type molecular structure. Raman spectra of the other B and C series have also been examined. For the spectra of the B2, B3 and B4 samples in the crystalline state, Raman bands characteristic of the trans-type B1 were found, while for those of the C2, C3 and C4 samples bands characteristic of the cis-type C1 appeared, as seen in Table 3. These observations reveal that the molecules of the B series take up a trans-type structure while those of the C-series adopt a cis-type structure in the crystalline state. Furthermore, as can be seen in Table 3, the Raman bands at 505–509 and 542–544 cm^{-1}, observed for the B series, closely correspond to the bands at 509 and 546 cm^{-1}, respectively, for the B1 sample, and those at 517–519 and 552–563 cm^{-1} for the C series also correspond to the bands at 519 and 553 cm^{-1}, respectively, of the C1 sample, indicating that these band frequencies can also be used to distinguish between the two conformations.

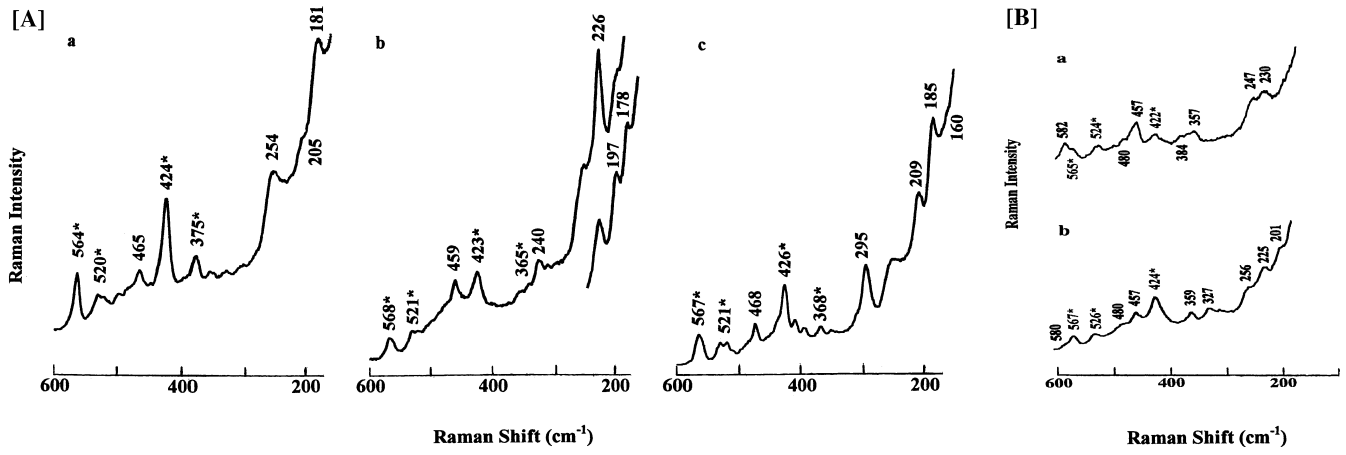

Fig. 5 A, B Raman spectra for the solid A series in the skeletal deformation region at **A** 25 °C (*a*: A1, *b*: A2, *c*: A3) and **B** at 60 °C (*a*: A1, *b*: A2). The *asterisked Raman bands* show the bands characteristic of the cis-type structure

Raman spectra of the A series and their conformations in the solid state

The Raman spectra (at 25 °C) in the skeletal deformation region of the crystalline samples for the A series are shown in Fig. 5A. It is found that the Raman bands at 423–425, 520 and 564–567 cm^{-1}, observed for all members of series correspond closely to those at 421–426, 517–519 and 552–563 cm^{-1}, respectively, which are characteristic of the cis-type C series. These observations imply that the A series systems with longer methylene spacers also take up a cis-type structure in the crystalline state. Therefore, these bands may be regarded as characteristics of the cis-type structure.

We may assume that an increase in temperature should bring about disordering of the skeletal structure of a polymethylene chain. In order to obtain information on disordering of the cis-type skeletal structure, we have measured the Raman spectra of the A series at higher temperatures.

The Raman spectra of the A1 and A2 samples in the crystalline state, measured at 60 °C are shown in Fig. 5B. For the A1 sample (Fig. 5A plot a, B plot a), it should be noted that an increase in temperature brings about both a marked decrease in intensity of the 423 cm^{-1} band and its broadening. Moreover, with increasing temperature, new bands at 230 and 580 cm^{-1} also appear and the very weak bands at 380 and 480 cm^{-1} become intensified. For the A2 sample (Fig. 5A plot b, B plot b), as the temperature increases, in addition to a broadening of the 424 cm^{-1} band, the broad band at about 480 cm^{-1} increases in intensity and a new band appears at 580 cm^{-1}. Similar observations were made for the A3 sample (spectrum at 60 °C not shown). These results suggest a breaking up of the cis-type structure and an increase in randomness of the *n*-alkyl chains.

Raman bands at 198–208 cm^{-1} are observed for all these DS in the crystalline state. We may assign these bands to the accordion modes of the spacer portion $[(CH_3)_2N^+—(CH_2)_6—N^+(CH_3)_2]$ in the A series. In order to confirm this assignment, the Raman spectra of HMB and its related compounds (TMDH and D_0) were measured. As shown in Fig. 6, strong Raman bands at 208, 198 and 200 cm^{-1} are observed for TMDH (Fig. 6b), HMB (Fig. 6c) and D_0 (Fig. 6d), respectively. We may assign these bands to the accordion modes of the TMDH segment.

The accordion vibrational mode of the TMDH portion for the A series is very close to that (194 cm^{-1}) of *n*-dodecane. An explanation for this similarity follows.

In the crystal structure of HMB (dihydride), which has been determined by X-ray diffraction analysis [32], the molecular chain $[CH_3—N(CH_2)_6N—CH_3]$ containing the nitrogen atom and one CH_3 carbon atom of the $N(CH_3)_3$ groups is in the fully extended state, although both $CN(CH_3)_3$ groups are slightly twisted out of the average plane of the $(CH_2)_6$ segment. Therefore, the all-trans plane should provide an accordion band frequency very close to that of *n*-decane [30]. However, we must consider that this segment contains two nitrogen atoms and that, furthermore, each nitrogen atom is linked with the methyl group. It is likely that these effects give rise to the appearance of the accordion mode at the lower frequency. The effect of substituent groups on the accordion band frequency has already been reported by Okabayashi and coworkers [18–23].

For the liquid sample of TMHD (Fig. 6a), a Raman band is also observed at 208 cm^{-1}, which corresponds well to the 208 cm^{-1} band of crystalline TMHD (Fig. 6b), indicating that the extended molecular structure of TMHD exists even in the liquid state.

The Raman spectra of *n*-alkyltrimethylammonium bromides in the crystalline state were also investigated in order to examine the accordion vibrations of the

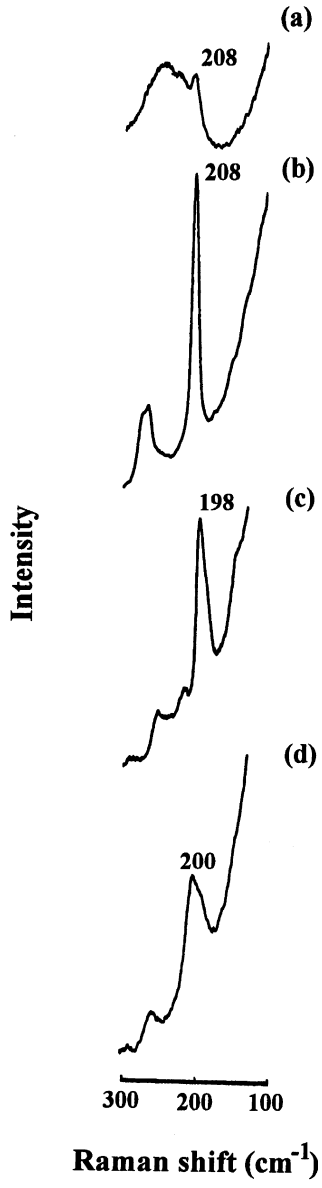

Fig. 6 Raman spectra of [tetramethyldiaminhexane **a** liquid and **b** solid (−60 °)], **c** solid hexamethonium bromide and **d** D_0 in the 100–300 cm^{-1} region

n-alkyl-N segments of the A series. The Raman spectra of *n*-hexyl, *n*-octyl, *n*-decyl and *n*-dodecyl trimethylammonium bromides in the 150–600 cm^{-1} region are shown in Fig. 7. It is seen that the strong Raman bands, which are observed for all in the 150–300 cm^{-1} region, are shifted markedly to lower frequency with an increase in the *n*-alkyl chain length. A similar observation was made by Mizushima and Simanouchi [30] for the Raman spectra of *n*-paraffins (C4–C16). They found that in the lower-frequency region only one Raman line exists for each solid paraffin and that its frequency is inversely proportional to the number of carbon atoms. This result

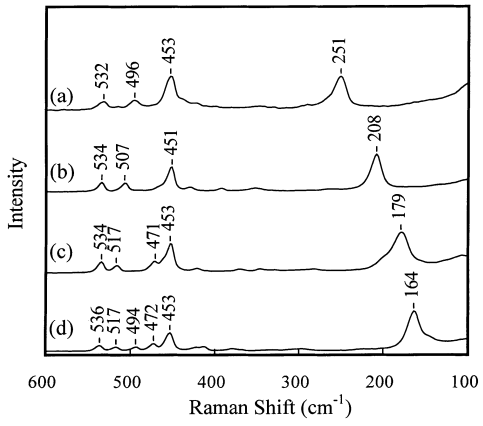

Fig. 7 Raman spectra for solid *n*-alkyltrimethylammonium bromides (**a** *n*-hexyl, **b** *n*-octyl, **c** *n*-decyl, **d** *n*-dodecyl) in the 150–600 cm^{-1} region (25 °C)

was accounted for by approximating the extended carbon chain as a continuous rod and assigning the Raman line to its longitudinal motion, the frequency of which is given by

$$\nu = \frac{1}{2\ell}\sqrt{\frac{E}{\rho}},$$

where E is Young's modulus, ρ the density and ℓ the length of the rod. This equation implies that the frequency is inversely proportional to the length of the hydrocarbon chain (number of carbon atoms). Thus, the Raman bands at 251, 208, 179 and 163 cm^{-1} (Fig. 7) can be assigned to the longitudinal vibrational modes (so-called accordion vibrational modes) of the *n*-hexyl, *n*-octyl, *n*-decyl and *n*-dodecyl chains, respectively. These bands are observed at lower frequencies than the accordion band frequencies of *n*-paraffins [30]. It is expected that the effect of the terminal groups (trimethylammonium ion) will contribute to this trend.

Figure 8 shows the linear relationship between the accordion band frequency and the reciprocal number of carbon atoms ($1/C_N$) for the DS and these values for the *n*-paraffins are included for comparison [30]. For A1, A2 and A3, therefore, we may assume that the accordion band frequencies of the *n*-octyl, *n*-decyl and *n*-dodecyl chains are very close to those of the *n*-alkyltrimethylammonium bromides. The Raman bands observed at 205, 178 and 160 cm^{-1} (Fig. 5A) for A1, A2 and A3 may be assigned to the accordion bands of the *n*-octyl, *n*-decyl and *n*-dodecyl chains.

Raman spectra of the A series-H_2O binary systems and the phase structures

The Raman spectra in the skeletal deformation region of the A series-H_2O binary systems are shown in Fig. 9.

For the aqueous solutions of A1 and A2 (Fig. 9A plot a, B plot a, respectively), the Raman bands observed at 423–424 cm^{-1} in the solid samples (Fig. 5) have disappeared, indicating that the cis-type structure which exists in the solid state has broken down in aqueous solution. Furthermore, the appearance of the very weak and broad bands at 365–370, 480 and 580 cm^{-1} implies disordering of the skeletal structure of these DS in aqueous solution. However, the presence of the weak bands at 513–515 cm^{-1} may imply the existence of a trans-type structure, since these bands correspond to the 509 cm^{-1} band (Fig. 6A) of the trans-type B1 molecule.

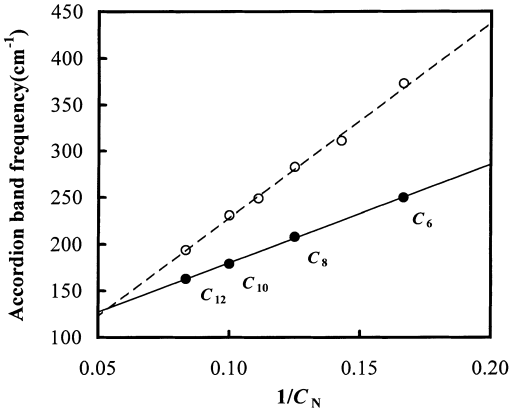

Fig. 8 Plots of the accordion band frequency against the reciprocal number ($1/C_N$) of carbon atoms for *n*-alkyltrimethylammonium bromides [*filled circles*: C_6 (*n*-hexyl), C_8 (*n*-octyl), C_{10} (*n*-decyl), C_{12} (*n*-dodecyl) and *open circles*: *n*-paraffins [31] (from *n*-hexane to *n*-dodecane)]

The Raman spectra of the A1 and A2 samples in the transparent gel state (Fig. 9A plot b, B plot b) are very similar to those seen in aqueous solution, again suggesting that the cis-type structure for the skeleton of these DS is broken in the gel state.

For the samples in the coagel states (Fig. 9A plot c, B plot c), the spectral features were found to be very similar to those of the aqueous and gel samples, although the broad bands at 465–468 cm^{-1} were increased in intensity. Therefore, we may assume that the cis-type structure of the skeleton is also broken in the coagel state.

Mizushima and Shimanouchi [30] investigated the Raman scattering of *n*-paraffins and concluded that while for the lower homologs (from *n*-butane to *n*-dodecane) the all-trans (extended) form is abundant in the liquid state, for *n*-cetane this form is almost absent

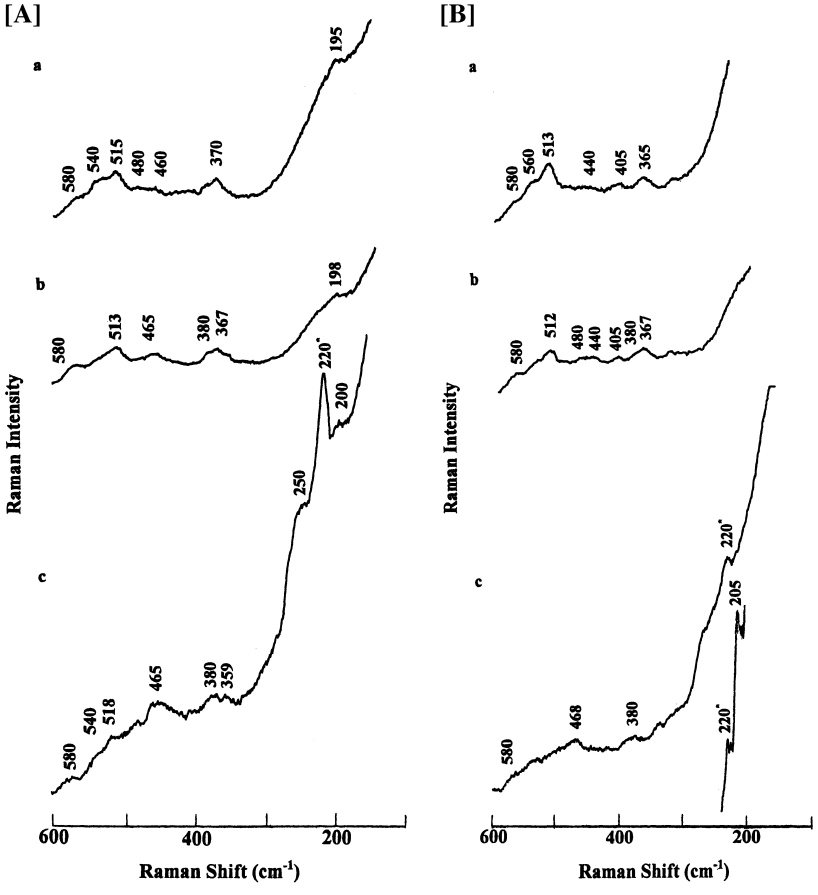

Fig. 9A, B Raman spectra for the A series-H_2O binary systems in the skeletal deformation region. **A**; Al-H_2O [*a*: aqueous solution (60 wt%, 25 °C), *b*: transparent gel (85 wt%, 25 °C), *c*: coagel (60 w%, −40 °C)], and **B**; A2-H_2O [*a*: aqueous solution (40 wt%, 25 °C), *b*: transparent gel (69 wt%, 60 °C), *c*: coagel (60 wt%, −40 °C)]. The *asterisked Raman bands* at 220 cm^{-1} are derived from the solid H_2O molecules

in that state. Okabayashi et al. [18] used Raman scattering of simple soap molecules in aqueous solution to demonstrate that the extended form of the hydrocarbon chain increases in population upon micellization. For A1 and A2 we may expect the appearance of the accordion bands for hexamethylenediamine, *n*-octyl, *n*-decyl and *n*-dodecyl chains in aqueous solution and in the gel and coagel states. For the aqueous, gel and coagel samples of A1, weak and broad bands at 195–198 cm^{-1} are observed (Fig. 9A plot a, b). These bands may probably be assigned to the accordion mode of the hexamethylenediamine chain, which was superimposed upon that of the *n*-octyl chain. For the coagel A2 sample, the band at 205 cm^{-1} (Fig. 9B plot c) may be assigned to the accordion mode of the spacer. The accordion band of the *n*-decyl chains could not be observed due to the presence of the very strong Rayleigh line. These observations reveal that the extended form of the spacer chain exists in all of the aqueous, gel and coagel states. Unfortunately, it is difficult to discuss the ordering state of the *n*-alkyl chains using the accordion modes. However, judging from the results of our previous work [24], we may assume that the *n*-alkyl chains are also in an extended form in the coagel state.

We can discuss the stability of the all-trans form in each phase using the skeletal stretching modes in the 1000–1100 cm^{-1} region. For the Raman scattering spectra of *n*-paraffins in the solid state, bands at 1056–1070 cm^{-1} are observed and are assigned to the skeletal (C—C) stretch modes of the extended form [31, 33]. However, for those of the *n*-paraffins in the liquid state, Raman bands at 1080–1086 cm^{-1} are found in addition to those at 1056–1070 cm^{-1}, and are assigned to the skeletal stretch modes of the conformers containing the gauche forms [33]. These results have been used extensively to examine the conformation of lipid molecules in model membranes and of surfactants in aggregated systems. We may use these bands in order to examine the phase structures of the A series-H_2O binary systems.

The Raman spectra of the solid A series in the 1000–1100 cm^{-1} region consist mainly of three bands (Table 2). The Raman bands at 1065–1067 cm^{-1} increased in intensity with increase in methylene number, compared with those at 1028–1030 and 1080–1081 cm^{-1}. This observation shows that the 1065–1067 cm^{-1} bands arise from the all-trans form of the *n*-alkyl chains. In order to assign the two bands at 1028–1030 and 1080–1081 cm^{-1}, the Raman spectrum of HMB in the crystalline state was also investigated in this study (spectra not shown) and three medium bands at 1026, 1061 and 1083 cm^{-1} were observed in this region. Therefore, we may assume that the three bands at 1028–1030, 1065–1067 and 1080–1081 cm^{-1} for the solid A series are superimposed upon the three bands arising from the extended hexamethonium skeleton.

The Raman spectra in the skeletal stretch region for the aqueous, transparent gel and coagel samples of the A1- and A2-H_2O binary systems are shown in Fig. 10. For A1, the Raman spectra of the aqueous and gel samples (Fig. 10A plot c, b, respectively) consist of two Raman bands at 1066–1069 and 1077–1080 cm^{-1}, indicating that the extended forms of the hydrocarbon chains are also abundant in the two phases and, as expected, are strongly dependent upon concentration. In the coagel state (Fig. 10A plot a), the 1068 cm^{-1} band is intensified compared with the band at 1079 cm^{-1}, indicating stabilization of the all-trans forms for the *n*-alkyl chains and the spacer segment. The Raman spectrum of A2 in aqueous solution (Fig. 10B plot c) is very similar to that of the transparent gel (Fig. 10B plot b) and bands at 1065–1068 and 1077–1079 cm^{-1} are observed. However, the latter bands are more intense than the former, indicating that the populations of conformers having a gauche form are predominant. For the Raman spectrum of A2 in the coagel state (Fig. 10B plot a), the two bands at 1066 and 1082 cm^{-1} are

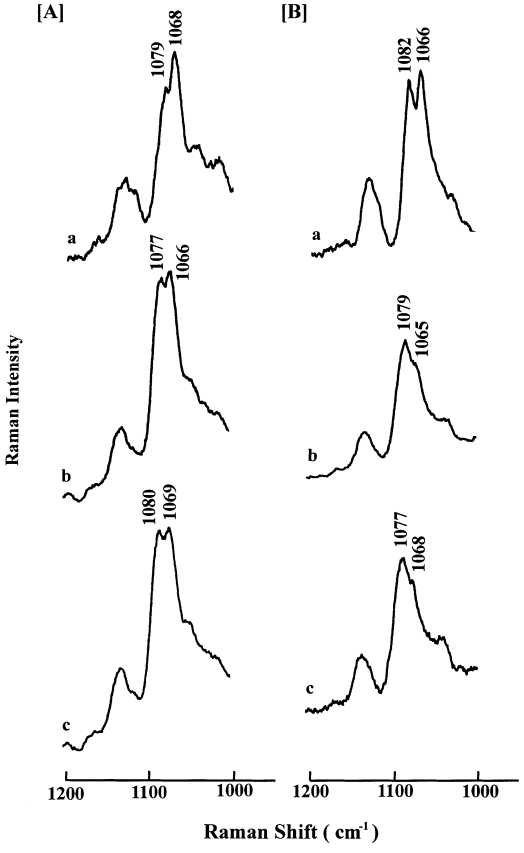

Fig. 10 A, B Raman spectra for the **A** Al-H_2O binary systems [*a*: coagel (60 wt%, −40 °C), *b*: transparent gel (80 wt%, 25 °C) and *c*: aqueous solution (80 wt%, 70 °C)] and **B** for the A2-H_2O [*a*: coagel (69 wt%, −40 °C), *b*: transparent gel (70 wt%, 60 °C) and *c*: aqueous solution (60 wt%, 25 °C)] in the skeletal stretch region

obviously intensified. Therefore, the all-trans forms of the hydrocarbon chains are preferentially stabilized. However, the presence of the medium and sharp 1082 cm^{-1} band may imply the presence of a considerable number of disordered hydrocarbon chains in the coagel phase.

Unfortunately, it is difficult to discuss the difference in the extent of ordering between the spacer chain and the *n*-acyl chains using Raman spectra in the accordion and skeletal stretch modes. In general, however, as the number of carbon atoms in *n*-paraffins decreases, the probability for taking up an all-trans form becomes high. Raman spectra of *n*-paraffins [30] and those of simple soap molecules [18, 19] support this assumption. Therefore, in solution, as well as in the transparent gel and coagel states, it may be assumed that the population of the all-trans form is greater in the spacer portion [N—$(CH_2)_6$—N] than in the acyl chains.

The CH_2 scissoring bands observed in the 1400–1500 cm^{-1} region are sensitive to molecular interactions and are useful as a monitor of the packing state of the methylene chains in the gel or crystalline state [34, 35]. In the Raman spectra of the A series, strong bands at 1441–1448 and 1455–1458 cm^{-1} are observed in this region (Table 2). It should be noted that an increase in the acyl chain length brings about a marked variation in this spectral feature. The separations (Dn) between the two bands become larger with an increase in the length of the acyl chain: Dn = 7 cm^{-1} for A1, 15 cm^{-1} for A2, and 16 cm^{-1} for A3. This behavior must be a reflection of the variation in the packing of the acyl chains upon an increase in the length of the acyl chain.

A similar observation has been made (data not shown) for the coagel samples of the A2-H_2O binary system. The Dn value for the coagel (40.3 wt%) A2 sample was 5 cm^{-1}, while for the 80 wt% coagel it was 14 cm^{-1} and very close to the value in the solid. This difference in Dn may reflect the difference in chain packing between the two coagel states, caused by the extent of hydration about the polar head groups. For the coagel samples of A1, such a splitting in this region was not observed, implying that the molecular packing state of the DS in the binary system depends on the length of the acyl chain.

For the gel samples of A1 and A2 (Fig. 10A plot b, B plot b, respectively), the spectral features the CH_2 scissoring modes were very similar to those of the aqueous samples. This may reflect the absence of molecular packing due to disordering of the hydrocarbon chains.

The relative intensities of C—H stretching bands have provided information about the ordering and the environment of the hydrocarbon moiety of phospholipids [36–38] and surfactant molecules [18, 39] in model membranes. In the present study, it has been found that the Raman spectral feature of the C—H stretch modes reflects the phase structure of the A series-H_2O binary systems. The Raman spectra for the solid A series in the C—H stretch region, observed at 25 °C and 60 °C, is shown in Fig. 11. The weak Raman bands in the 3000–3040 cm^{-1} region may arise from the N—CH_3 groups, since these bands decrease in intensity with an increase in the acyl carbon chain length (Fig. 11C < B < A). Moreover, the very strong Raman band at 3017 cm^{-1} and the medium 3038 cm^{-1} bands were also found in the Raman spectrum of solid HMB (spectrum not shown). The Raman bands at 2860–2865 and 2950–2952 cm^{-1} tend to decrease in intensity with an increase in the acyl carbon chain length (Fig. 11C < B < A) and correspond to the bands at 2856–2865 and 2957–2961 cm^{-1}, which were found for the Raman spectra of potassium *n*-alkylcarboxylates in the solid state, and are assigned to the terminal CH_3 groups of the acyl chains. The bands at 2886 cm^{-1} for A3 (Fig. 11C plot a) and that at 2902 cm^{-1} for A1 (Fig. 11A plot a) probably correspond to the 2880–2894 cm^{-1} band of potassium soap molecules in the solid state, which has often been used to discuss the ordering of hydrocarbon chains. The frequency of the Raman band characteristic of the solid state becomes higher as the temperature increases [2907 cm^{-1} for A1 (Fig. 11A plot b), 2892 cm^{-1} for A2 (Fig. 11B plot b) and 2894 cm^{-1} for A3 (Fig. 11C plot b)]. Furthermore, the Raman bands at 2929–2930 cm^{-1} (Fig. 11A plot b, B plot b, C plot b) are found to increase in intensity. These observations imply the presence of disordered hydrocarbon chains.

The Raman spectra of the aqueous solution, gel and coagel samples in the C—H stretch region are shown in Fig. 12. For the solution sample of A1 (Fig. 12A plot c), a very strong Raman band at 2936 cm^{-1} is observed,

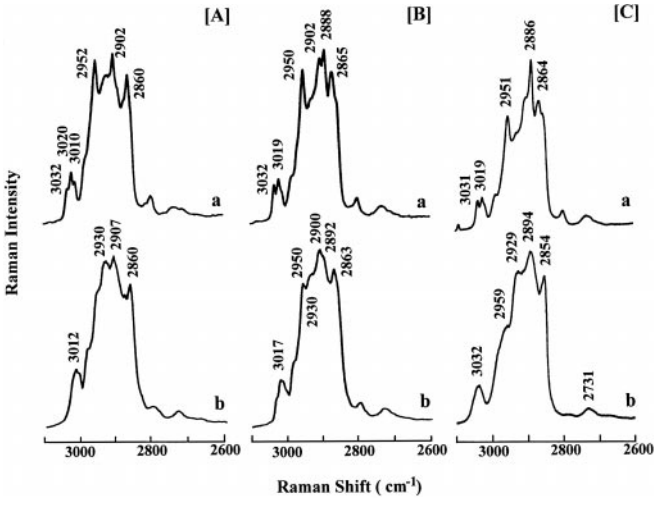

Fig. 11 A–C Raman spectra for the solid A series in the CH stretch region [**A** A1 (*a*: 25 °C, *b*: 60 °C), **B** A2 (*a*: 25 °C, *b*: 60 °C) and **C** A3 (*a*: 25 °C, *b*: 60 °C)]

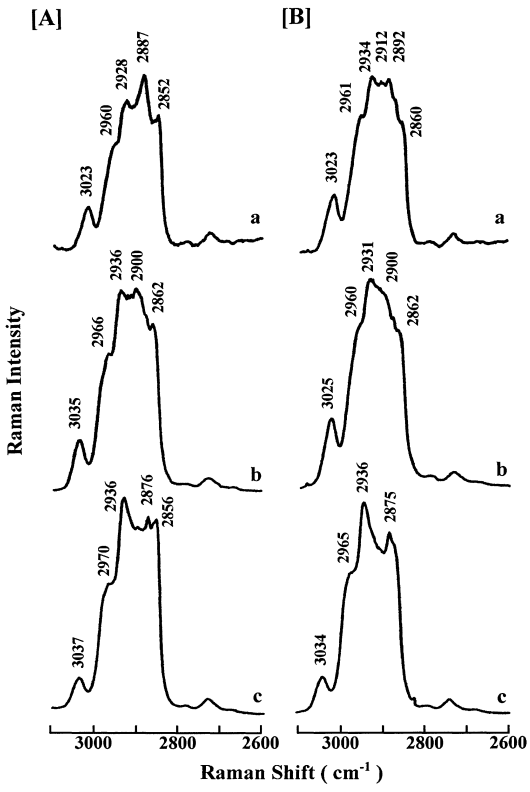

Fig. 12 A, B Raman spectra for the aqueous solution, gel and coagel samples of **A** A1 [*a*: coagel (79 wt%, −40 °C), *b*: transparent gel (85 wt%, 25 °C) and *c*: aqueous solution (60 wt%, 25 °C)] and of **B** A2 [*a*: coagel (69 wt%, −40 °C), *b*: transparent gel (70 wt%, 60 °C) and *c*: aqueous solution (60 wt%, 25 °C)]

reflecting preferential disordering of the hydrocarbon chains. However, for the gel sample (Fig. 12A plot b), a 2900 cm^{-1} band, as well as the 2936 cm^{-1} band, is found. This observation may reveal the presence of ordering of hydrocarbon chains in the gel state. The 2887 cm^{-1} band characteristic of the solid state appears in the spectrum of the coagel sample (Fig. 12A plot a). This observation may reflect an increase in the extent of ordering of hydrocarbon chains with an increase in population of the all-trans form. However, the appearance of the 2928–2936 cm^{-1} band for these three samples (Fig. 12A), corresponding to the 2930–2936 cm^{-1} band characteristic of the molten state [40], may indicate the introduction of disordered hydrocarbon chains brought about by the increase in temperature.

It has already been discussed that the overtones of the CH_2 scissoring fundamental mode play an important role in the Raman intensity around 2900 cm^{-1} [41]. In fact, in the Raman spectrum of the solid A1 sample, the CH_2 scissoring modes are observed at 1445 and 1455 cm^{-1} (Table 2), and the frequency (2890 cm^{-1}) of the overtone of the 1445 cm^{-1} band is very close to that of the 2887 cm^{-1} band (Fig. 12A plot a). Therefore, the intensity of the 2887 cm^{-1} band for the coagel sample may be largely due to intensity enhancement through Fermi resonance between the CH_2 symmetric stretch fundamental and the overtone mode.

Similar observations were made for the A2 samples in the aqueous, transparent gel and coagel states. In particular, it should be noted that the 2892 cm^{-1} band, corresponding to the 2888 cm^{-1} band of the solid, and the 2912 cm^{-1} band were observed for the coagel samples (Fig. 12B plot a). Since the CH_2 scissoring modes appear at 1443 and 1458 cm^{-1} in the solid state, we may expect that the overtone modes should appear at 2886 and 2916 cm^{-1} (Fig. 12B plot a). These expected frequencies are very close to the observed frequencies at 2892 and 2912 cm^{-1}, leading to the possibility of Fermi resonance between the CH_2 stretch fundamental and the overtones.

Thus, the increase in intensity for the 2887 cm^{-1} band of the coagel A1 sample (Fig. 12A plot a) and that for the 2892 and 2912 cm^{-1} bands of the coagel A2 sample (Fig. 12B plot a) may be caused by molecular packing of the DS molecules due to an increase in concentration in the coagel phase.

Conclusion

The Raman scattering spectra of DS (A series) in the solid and various aqueous phases have been measured and compared with those of simple DS B1 and C1, whose molecular structures have been elucidated by single-crystal X-ray diffraction analysis. The results may be summarized as follows. For the DS molecules of the A series in the solid state, the molecular skeleton takes up a cis-type configuration similar to that of the C1 molecule, and their *n*-octyl, *n*-decyl and *n*-dodecyl chains in the solid state as well as the hexamethylene spacer are in a fully extended state. This skeletal cis configuration may be broken in various aqueous phases.

The skeletal stretching modes in the 1000–1100 cm^{-1} region suggest that the all-trans form for the *n*-alkyl chains and spacer segment is abundant in the aqueous and gel phases and, particularly in the coagel state, stabilization of the all-trans form for these polymethylenes becomes dominant.

Furthermore, it has been found that the CH_2 scissoring bands strongly reflect the packing state of the polymethylene chains for the DS in the gel or crystalline state and the C—H stretch bands provide information about the phase structure of the A series-H_2O binary system.

Acknowledgements The authors thank Hisatoshi Yamauchi, Motoi Mori, Tatsuya Uehama and Naoki Ichiyanagi for their assistance in the synthesis of the dimeric surfactants.

References

1. (a) Deinega YF, Ulberg ZR, Marochko LG, Rudi VP, Denisenko VP (1974) Kolloidn Zh 36:649–653; (b) Ul'berg ZR, Podolskaya VI (1978) Kolloidn Zh 40:292–296
2. Parreira HC, Lukenbach ER, Lindemann MKO (1979) J Am Oil Chem Soc 56:1015–1021
3. Devinsky F, Masarova L, Lacko I (1985) J Colloid Interface Sci 105:235–239
4. Devinsky F, Lacko I, Bitterova F, Tomeckova L (1986) J Colloid Interface Sci 114:314–322
5. Rozycka-Roszak B, Witek S, Przestalski S (1989) J Colloid Interface Sci 131:181–185
6. Devinsky F, Lacko I, Imam T (1990) Acta Fac Pharm Univ Comenianae 44:103–117
7. Devinsky F, Lacko I (1990) Tenside Surfactants Deterg 27:344–349
8. Devinsky F, Lacko I, Imam T (1991) J Colloid Interface Sci 143:336–342
9. Zana R, Benrraou M, Rueff R (1991) Langmuir 7:1072–1075
10. Alami E, Levy H, Zana R, Skoulios A (1993) Langmuir 9:940–944
11. Abid SK, Hamid SM, Sherrington DC (1987) J Colloid Interface Sci 120: 245–255
12. Imam T, Devinsky F, Lacko I, Mlynarcik D, Krasnec L (1983) Pharmazie 38:308–310
13. Devinsky F, Lacko I, Mlynarcik D, Racansky V, Krasnec L (1985) Tenside Deterg 22:10–15
14. Zana R, Talmon Y (1993) Nature 362:228–230
15. Alami E, Beinert G, Marie P, Zana R (1993) Langmuir 9:1465–1467
16. Diamant H, Andelman D (1994) Langmuir 10:2910–2916
17. (a) Hirata H, Hattori N, Ishida M, Okabayashi H, Furusaka M, Zana R (1995) J Phys Chem 99:17778–17784; (b) Hattori N, Hirata H, Okabayashi H, Furusaka M, O'Connor CJ, Zana R (1998) Colloid Polym Sci (in press)
18. Okabayashi H, Okuyama M, Kitagawa T (1975) Bull Chem Soc Jpn 48:2264–2269
19. Okabayashi H, Abe M (1980) J Phys Chem 84:999–1005
20. Okabayashi H, Yoshida T, Terada Y, Ikeda T, Matsushita K (1981) Z Naturforsch A 36:1352–1356
21. Okabayashi H, Yoshida T, Ikeda T, Matsuura H, Kitagawa T (1982) J Am Chem Soc 104:5399–5402
22. Okabayashi H, Taga K, Tsukomoto K, Tamaoki H, Yoshida T, Matsuura H (1985) Chemica Scr 25:153–156
23. (a) Tsukamoto K, Ohshima K, Taga K, Okabayashi H, Matsuura H, (1987) J Chem Soc Faraday Trans 1 83:789–800 (b) Okabayashi H, Tsukamoto K, Ohshima K, Taga K, Nishio E (1988) J Chem Soc Trans 84:1639–1651
24. Okabayashi H, Taga K, Miyagai K, Uehara T, Yoshida T, Nishio E (1991) J Phys Chem 95:7932–7938
25. Taga K, Ohshima K, Matsuoka H, Yoshida T, Okabayashi H (1993) Colloids Surf A 81:59–64
26. Okabayashi H, Hirata H, Suzuki Y, Taga K, Mathew C (1996) Vib Spectrosc 10:239–251
27. Etori H, Yamada Y, Taga K, Okabayashi H, Ohshima K, O'Connor CJ (1997) Vib Spectrosc 14:133–141
28. Ikeda S, Hayashi S, Imae T (1981) J Phys Chem 85:106–112
29. Hattori N, Masuda H, Okabayashi H, O'Connor CJ (1998) J Mol Struct 47: 13–18
30. Mizushima S, Shimanouchi T (1949) J Am Chem Soc 71:1320–1324
31. Schaufele RF (1968) J Chem Phys 49:4168–4175
32. Lonsdale K, Milledge HJ, Pant LM (1965) Acta Crystallogr 19:827–840
33. Snyder RG, Schachtshneider JH (1963) Spectochim Acta 19:85–116
34. Snyder RG (1967) J Chem Phys 47:1316–1360
35. Kawai T, Umemura J, Takenaka T, Kodama M, Seki S (1985) J Colloid Interface Sci 103:56–61
36. Brown KG, Peticolas WL, Brown E (1973) Biochem Biophys Res Commun 54:358–364
37. Gaber BP, Peticolas WL (1977) Biochim Biophys Acta 465:260–274
38. Larsson K (1973) Chem Phys Lipids 10:165–176
39. Okabayashi H, Okuyama M, Kitagawa T, Miyazawa T (1974) Bull Chem Soc Jpn 47:1075–1077
40. Lippert JL, Peticolas WL (1971) Proc Natl Acad Sci USA 68:1572–1576
41. Okabayashi H, Kitagawa T (1978) J Phys Chem 82:1830–1836